Journal of Solid Mechanics Vol. 12, No. 2 (2020) pp. 366-384
DOI: 10.22034/jsm.2019.1866762.1428

Analytical Stress Solutions of an Orthotropic Sector Weakened by Multiple Defects by Dislocation Approach

A.R. Hassani *, A. Hassani

Young Researchers and Elite Club, Hashtgerd Branch, Islamic Azad University, Alborz, Iran

Received 3 March 2020; accepted 27 April 2020

ABSTRACT

In this article, the anti-plane deformation of an orthotropic sector with multiple defects is studied analytically. The solution of a Volterra-type screw dislocation problem in a sector is first obtained by means of a finite Fourier cosine transform. The closed form solution is then derived for displacement and stress fields over the sector domain. Next, the distributed dislocation method is employed to obtain integral equations of the sector with cracks and cavities under anti-plane traction. These equations are of Cauchy singular kind, which are solved numerically by generalizing a numerical method available in the literature by means of expanding the continuous integrands of integral equations with different weight functions in terms of Chebyshoff and Jacobi polynomials. A set of examples are presented to demonstrate the applicability of the proposed solution procedure. The geometric and force singularities of stress fields in the sector are also studied and compared to the earlier reports in the literature.

Keywords : Anti-plane; Sector; Orthotropic; Stress intensity factor; Hoop stress.

1 INTRODUCTION

THE stress analysis of wedges and sectors has been considered by a number of earlier investigators. These investigations may be grouped into two major categories: those primarily dealing with wedges and sectors with no defects, and those studying wedges and sectors with single or multiple defects. Within the first category, the problem of anti-plane stress analysis of an isotropic and dissimilar finite wedge, with different boundary conditions under point tractions on the wedge straight edges, was originally studied by Kargarnovin, Shahani and Fariborz [1] and Kargarnovin and Fariborz [2]. A finite Mellin transform was used to analyze the wedge problem, and subsequently the geometric and loading singularities were investigated. Similarly, the stress analysis of an anisotropic finite wedge under anti-plane deformation was studied by Shahani [3]. Using the above-mentioned stress field and changing only the apex angle of finite wedge, the stress intensity factor (SIF) due to an edge crack in circular shafts and also the stress concentration factor in the apex of bonded wedges as well as bonded half planes were evaluated. More recently, the stress concentration factor for a double cantilever beam (DCB) was extracted by

*Corresponding author. Tel.: +98 26 442 0163.
E-mail address: ahassani1111@gmail.com (A.R.Hassani).

Shahani [4]. Solutions of dissimilar isotropic wedges subjected to anti-plane point forces and screw dislocations were studied by Lin and Ma [5] using the Mellin transform and an image method. It was assumed that wedges with equal apex angles are attached to each other along their interface. Various boundary conditions on the wedge edges were considered and with the aid of the Peach–Koehler equation, the stress field of the image forces exerted on screw dislocations was derived. The solution of an isotropic sector wedge subjected to anti-plane shear loading on a circular edge of the wedge was obtained by Chen and Wang [6]. Different boundary conditions including fixed and traction free conditions were considered for straight edges of the finite wedge. A combination of the finite Mellin transform and the Laplace transform was used to solve the ensuing governing equations. Finally, the stress concentration of the wedge apex was studied for different edge boundary conditions. Wedges and sectors weakened by multiple defects have been the subject of other earlier investigations. The anti-plane stress analysis of an infinite wedge weakened by a finite number of collinear cracks located on the wedge bisector was first studied by Mkhitaryan, Melkoumian and Lin [7]. The anti-symmetric mixed boundary conditions on both wedge faces were the specified displacement and stress components on the nonintersecting intervals. A closed-form solution of the ensuing mixed boundary problem was derived using the Mellin integral transformation in conjunction with the singular integral equations, and the crack opening and SIF on cracks tips were calculated. Anti-plane stress analysis of an infinite wedge weakened by multiple cracks with an arbitrary smooth shape and orientation was also investigated by Faal, Fotuhi, Fariborz and Daghyani [8]. The Mellin transform was used to solve the problem and the stress field of an uncracked wedge under point traction on the wedge edges was obtained. In another report by [9], the Mellin transform in conjunction with an image method was used to analyze the anti-plane stress field of a finite wedge weakened by multiple cavities. Similarly, the stress field of an undamaged finite wedge under concentrated traction on the edges was attained. In both aforementioned works, various types of boundary conditions were considered. Anti-plane stress analysis of an anisotropic finite wedge weakened by a single radial crack was the subject of the study by [10]. The governing equation of the problem was rewritten in a complex form by introducing appropriate complex variables, and the solution was obtained in terms of complex functions using a set of finite complex transformations (also see [3, 11]). The latter complex method may be analogous to the standard finite Mellin transforms of the first and second types. The ensuing singular dual integral equations were solved numerically to calculate the stress intensity factors at the wedge crack tips. The anti-plane stress analysis of two different types of dissimilar sectors, i.e. the sector consisting of two isotropic sectors with the circular or the radial interface, was accomplished by [12]. Using the finite Fourier cosine transform as well as the technique of separation of variables, the closed-form solutions were obtained for the displacement and stress fields in each sector. Anti-plane deformation of a typical dissimilar sector, consisting of two sub-sectors with a circular interface, was the subject of study by [13]. Using the finite Fourier cosine transform, the exact closed-form solutions for the displacement and stress fields of a Volterra type screw dislocation were attained. Next, using a distributed dislocation method, singular integral equations of the dissimilar sector weakened by defects (located in one of the sub-sectors) were obtained. The governing equations were found to be of the Cauchy type and solved numerically. For the sector in [12], in comparison with [13], an additional boundary condition was chosen such that the finite Fourier cosine transform was no longer useful and the technique of separation of variables was employed. Moreover, a new dissimilar sector, namely with the radial interface, was analyzed.

According to the brief review above, the stress analysis of orthotropic sectors weakened by multiple, arbitrarily shaped defects and with two circular fixed edges has not been the subject of previous investigations. In this article, the classical theory of elasticity for the stress analysis of an orthotropic sector containing Volterra-type screw dislocations is first presented (Section 2). For the simplicity of dislocation solutions, we use the dislocation arc instead of dislocation line to define the dislocation. Results in Section 2 have been validated by available dislocation solutions of isotropic finite wedges in the literature. Next, the stress analysis of a sector under point and patch loading is studied for selected boundary conditions (Section 3). Similar to Section 2, results for special cases (namely, finite wedges) have been validated by the reported data in the literature. Methodologically, Buckner's principle can be used to analyze sectors weakened by multiple cracks and cavities using the results of Sections 2 and 3. This approach is shown in Section 4. Numerical examples are presented in Section 5 and results are compared to those of an isotropic infinite wedge. Concluding remarks are included in Section 6.

2 GENERAL FORMULATION

Let us consider an orthotropic sector (Fig. 1(a)) with inner and outer radii R_1 and R_2 and sector angle α. The origin of polar coordinate is located at the center of the sector circular edges and the angle θ is measured from the

lower edge. Such, the sector consists of two sub-sectors $R_1 \le r \le a$ and $a \le r \le R_2$ which are attached together along the circular arc $r = a$. The only nonzero displacement component under anti-plane deformation is the out of plane component $w\left(r,\theta\right)$ in each region.

The equilibrium equation in the absence of body forces in the polar coordinates is written as:

$$\frac{\partial \tau_{rz}}{\partial r} + \frac{1}{r}\frac{\partial \tau_{\theta z}}{\partial \theta} + \frac{\tau_{rz}}{r} = 0 \tag{1}$$

The constitutive equations for non-vanishing stress components are:

$$\tau_{rz} = G_{rz}\frac{\partial w}{\partial r} \qquad \tau_{\theta z} = G_{\theta z}\frac{1}{r}\frac{\partial w}{\partial \theta} \tag{2}$$

where G_{rz} and $G_{\theta z}$ are the orthotropic shear moduli of the sector ([14]). Substituting Eqs. (2) into Eq. (1) leads to

$$r^2\frac{\partial^2 w}{\partial r^2} + r\frac{\partial w}{\partial r} + G^2\frac{\partial^2 w}{\partial \theta^2} = 0 \tag{3}$$

where $G = \sqrt{\frac{G_{\theta z}}{G_{rz}}}$. Finite Fourier cosine transform for a sufficiently regular function $f\left(\theta\right)$ is defined as:

$$F(n) = \int_0^{\alpha} f\left(\theta\right)\cos\frac{n\pi\theta}{\alpha}d\theta \tag{4}$$

The inverse of finite Fourier cosine transform yields

$$f\left(\theta\right) = \frac{2}{\alpha}\sum_{n=1}^{\infty}F(n)\cos\frac{n\pi\theta}{\alpha} \tag{5}$$

The traction-free condition on the sector straight edges and also the fixed edge conditions at the edges $r = R_1$ and $r = R_2$ imply that

$$\begin{aligned} &\frac{\partial w\left(r,0\right)}{\partial \theta} = 0 && \frac{\partial w\left(r,\alpha\right)}{\partial \theta} = 0 \\ &w\left(R_1,\theta\right) = 0 && w\left(R_2,\theta\right) = 0 \end{aligned} \tag{6}$$

Application of finite Fourier cosine transform (4) into Eq. (3) and viewing the boundary conditions (6) leads to

$$r^2\frac{\partial^2 W\left(r,n\right)}{\partial r^2} + r\frac{\partial W\left(r,n\right)}{\partial r} - (n\kappa)^2 W\left(r,n\right) = 0 \tag{7}$$

where $\kappa = \frac{\pi G}{\alpha}$ .The general solution to Eq. (7) is obtained as:

$$W\left(r,n\right) = A_{kn}r^{n\kappa} + B_{kn}r^{-n\kappa}, k = 1,2 \tag{8}$$

Constants A_{kn} and B_{kn} should be determined by applying appropriate boundary and continuity conditions. The index k = 1, 2 is used to refer to the closer and farther sectors to the origin *O*, respectively (Fig. 1(a)). By virtue of Eqs. (5) and (8), the out of plane component $w\left(r,\theta\right)$ is written as:

$$w\left(r,\theta\right)=\frac{2}{\alpha}\sum_{n=1}^{\infty}(A_{kn}r^{n\kappa}+B_{kn}r^{-n\kappa})cos\,\frac{n\pi\theta}{\alpha},\ \ k=1,2 \tag{9}$$

A Volterra type screw dislocation with Burgers vector δ is situated at the point (a,β) with the dislocation arc $r=a, 0\le\theta\le\beta$. Here we use dislocation arc instead of dislocation line (see [8, 9]) to define the dislocation. The boundary condition representing an arc dislocation under anti-plane deformation reads

$$w\left(a^{-},\theta\right)-w\left(a^{+},\theta\right)=\delta H\left(\beta-\theta\right) \tag{10}$$

where H is the Heaviside step function. The continuity condition (self-equilibrium of stress) in the sector containing the dislocation as follows.

$$\tau_{rz}\left(a^{+},\theta\right)=\tau_{rz}\left(a^{-},\theta\right) \tag{11}$$

Appling the finite Fourier cosine transform to Eqs. (10) and (11) results in

$$\begin{aligned}&W\left(a^{-},n\right)-W\left(a^{+},n\right)=(\delta\alpha/n\pi)\sin(n\pi\beta/\alpha)\\&\frac{\partial W\left(a^{+},n\right)}{\partial r}-\frac{\partial W\left(a^{-},n\right)}{\partial r}=0\end{aligned} \tag{12}$$

The first pair of boundary conditions (6) is readily satisfied and applying the second pair of boundary conditions (6) to Eqs. (9) gives

$$A_{1n}R_1^{n\kappa}+B_{1n}R_1^{-n\kappa}=0 \qquad A_{2n}R_2^{n\kappa}+B_{2n}R_2^{-n\kappa}=0 \tag{13}$$

Application of the conditions (12) to Eq. (9) leads to

$$\begin{aligned}&(A_{1n}a^{n\kappa}+B_{1n}a^{-n\kappa})-(A_{2n}a^{n\kappa}+B_{2n}a^{-n\kappa})=(\delta\alpha/n\pi)\sin(n\pi\beta/\alpha)\\&(A_{1n}a^{n\kappa}-B_{1n}a^{-n\kappa})-(A_{2n}a^{n\kappa}-B_{2n}a^{-n\kappa})=0\end{aligned} \tag{14}$$

Solution of Eqs. (13) and (14) gives

$$\begin{aligned}A_{1n}&=(\delta\alpha/2\pi)a^{-n\kappa}(\left(a/R_2\right)^{2n\kappa}+1)\Lambda_{\mathrm{n}}\\B_{1n}&=-(\delta\alpha/2\pi)(R_1^2/a)^{n\kappa}(\left(a/R_2\right)^{2n\kappa}+1)\Lambda_{\mathrm{n}}\\A_{2n}&=(\delta\alpha/2\pi)a^{-n\kappa}(\left(a/R_2\right)^{2n\kappa}+(R_1/R_2)^{2n\kappa})\Lambda_{\mathrm{n}}\\B_{2n}&=-(\delta\alpha/2\pi)(a^{n\kappa}+(R_1^2/a)^{n\kappa})\Lambda_{\mathrm{n}}\end{aligned} \tag{15}$$

where $\Lambda_{\mathrm{n}}=\sin(n\pi\beta/\alpha)/n\left(1-(R_1/R_2)^{n\kappa}\right)$. Substituting coefficients (15) into Eqs. (9) results in:

$$\begin{aligned}w\left(r,\theta\right)&=\frac{\delta}{\pi}\sum_{n=1}^{\infty}\Lambda_{\mathrm{n}}[(r/a)^{n\kappa}+\left(ra/R_2^2\right)^{n\kappa}-(aR_1^2/rR_2^2)^{n\kappa}-(R_1^2/ra)^{n\kappa}]cos\,\frac{n\pi\theta}{\alpha} \qquad R_1\le r\le a\\w\left(r,\theta\right)&=\frac{\delta}{\pi}\sum_{n=1}^{\infty}\Lambda_{\mathrm{n}}[\left(ra/R_2^2\right)^{n\kappa}+(rR_1^2/aR_2^2)^{n\kappa}-(a/r)^{n\kappa}-(R_1^2/ra)^{n\kappa}]cos\,\frac{n\pi\theta}{\alpha} \qquad a\le r\le R_2\end{aligned} \tag{16}$$

Using the first Eq. (16) in Eq. (2), the stress field when, $R_1\le r\le a$ is obtained as:

$$\tau_{rz} = GG_{rz}\frac{\delta}{\alpha r}\sum_{n=1}^{\infty} n\Lambda_n[(r/a)^{n\kappa} + \left(ra/R_2^2\right)^{n\kappa} + (aR_1^2/rR_2^2)^{n\kappa} + (R_1^2/ra)^{n\kappa}]cos\,\frac{n\pi\theta}{\alpha}$$
$$\tau_{\theta z} = -G_{\theta z}\frac{\delta}{\alpha r}\sum_{n=1}^{\infty} n\Lambda_n[(r/a)^{n\kappa} + \left(ra/R_2^2\right)^{n\kappa} - (aR_1^2/rR_2^2)^{n\kappa} - (R_1^2/ra)^{n\kappa}]sin\,\frac{n\pi\theta}{\alpha} \quad (17)$$

For $a \le r \le R_2$ the stress component $\tau_{rz}(r,\theta)$ is achieved by replacing r/a with a/r. Analogously for stress component $\tau_{\theta z}(r,\theta)$, similar changes are made for each region. Moreover the changed parts are multiplied by a negative sign. Making use of the formulas given in the Appendix of the report by Faal, Fotuhi, Fariborz and Daghyani [8] and the Taylor's expansion of expression $n\Lambda_n$ (i.e., $\Lambda_n = \sin(n\pi\beta/\alpha)/n\left(1-(R_1/R_2)^{n\kappa}\right)$), the stress components (17) are summed in the whole sector region, leading to

$$\begin{aligned}
\tau_{rz} &= \frac{\delta\kappa G_{rz}}{4\pi r}\sum_{m=0}^{\infty}\{\left[\varphi_m\left(r/a,\pi(\beta-\theta)/\alpha\right)+\varphi_m\left(r/a,\pi(\beta+\theta)/\alpha\right)\right]\\
&+\left[\varphi_m\left(ra/R_2^2,\pi(\beta-\theta)/\alpha\right)+\varphi_m\left(ra/R_2^2,\pi(\beta+\theta)/\alpha\right)\right]\\
&+\left[\varphi_m\left(aR_1^2/rR_2^2,\pi(\beta-\theta)/\alpha\right)+\varphi_m\left(aR_1^2/rR_2^2,\pi(\beta+\theta)/\alpha\right)\right]\\
&+\left[\varphi_m\left(R_1^2/ra,\pi(\beta-\theta)/\alpha\right)+\varphi_m\left(R_1^2/ra,\pi(\beta+\theta)/\alpha\right)\right]\},\quad R_1 \le r \le a\\
\tau_{\theta z} &= -\frac{\delta\kappa G G_{rz}}{4\pi r}\sum_{m=0}^{\infty}\{\psi_m\left(r/a,\pi(\beta+\theta)/\alpha\right)-\psi_m\left(r/a,\pi(\beta-\theta)/\alpha\right)\\
&+\psi_m\left(ra/R_2^2,\pi(\beta+\theta)/\alpha\right)-\psi_m\left(ra/R_2^2,\pi(\beta-\theta)/\alpha\right)\\
&-\psi_m\left(aR_1^2/rR_2^2,\pi(\beta+\theta)/\alpha\right)+\psi_m\left(aR_1^2/rR_2^2,\pi(\beta-\theta)/\alpha\right)\\
&-\psi_m\left(R_1^2/ra,\pi(\beta+\theta)/\alpha\right)+\psi_m\left(R_1^2/ra,\pi(\beta-\theta)/\alpha\right)\},\quad R_1 \le r \le a
\end{aligned} \quad (18)$$

where $\eta = R_1/R_2$ and

$$\varphi_m(x,\theta,\kappa,\eta) = \frac{sin\,\theta}{\cosh(\kappa[2mLn\eta + Lnx]) - cos\,\theta}$$
$$\psi_m(x,\theta,\kappa,\eta) = \frac{\sinh\left(\kappa[2mLn\eta + Lnx]\right)\}}{\cosh\left(\kappa[2mLn\eta + Lnx]\right) - cos\,\theta} \quad (19)$$

For the sake of brevity, the constants κ and η were eliminated from Eqs. (18). For finite wedges, $R_1 = 0$ then $\eta = 0$ and the functions $\varphi_m(x,\theta,\kappa,\eta)$ and $\psi_m(x,\theta,\kappa,\eta)$ are vanished for all $m \ne 0$. Therefore, the stress field (18) is simplified for finite wedge as:

$$\begin{aligned}
\tau_{rz} &= \frac{\delta\kappa G_{rz}}{4\pi r}[\varphi_0\left(r/a,\pi(\beta-\theta)/\alpha\right)+\varphi_0\left(r/a,\pi(\beta+\theta)/\alpha\right)+\varphi_0\left(ra/R_2^2,\pi(\beta-\theta)/\alpha\right)\\
&+\varphi_0\left(ra/R_2^2,\pi(\beta+\theta)/\alpha\right)],\quad 0 \le r \le a\\
\tau_{\theta z} &= \frac{\delta\kappa G G_{rz}}{4\pi r}[-\psi_0\left(r/a,\pi(\beta+\theta)/\alpha\right)\\
&+\psi_0\left(r/a,\pi(\beta-\theta)/\alpha\right)-\psi_0\left(ra/R_2^2,\pi(\beta+\theta)/\alpha\right)+\psi_0\left(ra/R_2^2,\pi(\beta-\theta)/\alpha\right)],\quad 0 \le r \le a
\end{aligned} \quad (20)$$

Comparing the above stress field and that was obtained by Faal, Fariborz and Daghyani [9] after some manipulations shows identical results. It is also worth mentioning here that the dislocation definition used by Faal, Fariborz and Daghyani [9] was based on a straight cut of the wedge, but here we employ a circular cut to define the

dislocation. One of the benefits of the use of circular cut here is the simplicity of the finding the dislocation solutions. To investigate the behavior of stress fields in the dislocation position, let us change to a new coordinate system (ρ,ξ), (Fig. 1 (a)). The relationships between the two coordinates may be written as:

$$r=\sqrt{a^2+\rho^2+2a\rho\sin\xi},\theta=\beta-\sin^{-1}\left(\frac{\rho\cos\xi}{\sqrt{a^2+\rho^2+2a\rho\sin\xi}}\right)\quad,0\le\xi\le 2\pi \tag{21}$$

Substituting (21) into $\varphi_0\left(r/a,\pi(\beta-\theta)/\alpha\right)$ and $\psi_0\left(r/a,\pi(\beta-\theta)/\alpha\right)$ and carrying out the necessary manipulations yields

$$\begin{aligned}&\frac{1}{r}\varphi_0\left(r/a,\pi(\beta-\theta)/\alpha\right)\sim\frac{2\alpha}{\pi\cos\xi}\frac{1}{\rho},\ \text{as}\ \rho\to 0,0\le\xi\le 2\pi\lim_{x\to\infty}\\&\frac{1}{r}\psi_0\left(r/a,\pi(\beta-\theta)/\alpha\right)\sim\frac{G\alpha\sin\xi}{2\pi\cos^2\xi}\frac{1}{\rho},\ \text{as}\ \rho\to 0,0\le\xi\le 2\pi\end{aligned} \tag{22}$$

According to the above relations one can conclude that $(\tau_{rz},\ \tau_{\theta z})\sim\frac{1}{\rho}$ as $\rho\to 0$. It should be added that this Cauchy singularity was previously reported, e.g., by Weertman, Friedel and Rhodes [15], for the stress field of two-dimensional isotropic media containing screw dislocations. It has also been reported by [8, 9] for the stress field of an orthotropic strip and rectangular containing screw dislocations.

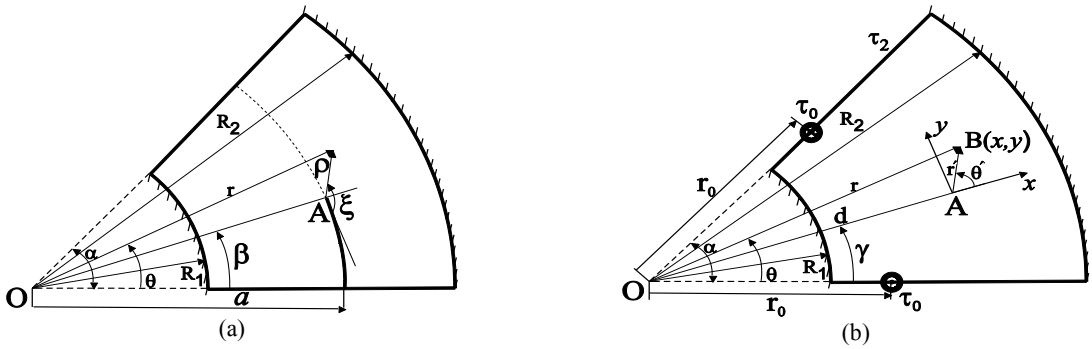

Fig.1
(a) Sector with screw dislocation, (b) Sector under anti-plane loading.

3 ORTHOYROPIC SECTOR UNDER TRACTION

In this section we use the analyses framework of Section 2 and predict the anti-plane deformation of an orthotropic sector under two point forces/tractions with a magnitude of τ_0. (Fig. 1(b)). The boundary conditions (6) hold but the first two boundary conditions are replaced by

$$\tau_{\theta z}\left(r,0\right)=\tau_{\theta z}\left(r,\alpha\right)=\tau_0\delta(r-r_0) \tag{23}$$

where $\delta(\ldots)$ is Delta Dirac function. Application of finite Fourier cosine transform (4) to Eq. (3) and viewing the boundary conditions (23) leads to

$$r^2\frac{\partial^2 W\left(r,n\right)}{\partial r^2}+r\frac{\partial W\left(r,n\right)}{\partial r}-\left(n\kappa\right)^2 W\left(r,n\right)=(r\tau_0/G_{\theta z})\left[1+(-1)^{n+1}\right]\delta(r-r_0) \tag{24}$$

Solving Eq. (24) as a Green function problem leads to seeking a $W\left(r,n\right)$ as follows:

$$\begin{cases} W\left(r,n\right)=C_1 r^{n\kappa}+D_1 r^{-n\kappa} R_1 \le r \le r_0 \\ W\left(r,n\right)=C_2 r^{n\kappa}+D_2 r^{-n\kappa} r_0 \le r \le R_2 \end{cases} \tag{25}$$

Continuity of displacements at $r=r_0$ imply that

$$W\left(r_0^-,n\right)=W\left(r_0^+,n\right) \tag{26}$$

Application of the last two boundary conditions (6) and continuity Eqs. (26) to (25) in view of (5) gives

$$\begin{aligned} &C_1 R_1^{n\kappa}+D_1 R_1^{-n\kappa}=0 \\ &C_2 R_2^{n\kappa}+D_2 R_2^{-n\kappa}=0 \\ &C_1 r_0^{n\kappa}+D_1 r_0^{-n\kappa}=C_2 r_0^{n\kappa}+D_2 r_0^{-n\kappa} \end{aligned} \tag{27}$$

Integrating Eq. (24) across the arc $r=r_0$ gives

$$\int_{r_0^-}^{r_0^+} r^2 \frac{\partial^2 W\left(r,n\right)}{\partial r^2} dr+\int_{r_0^-}^{r_0^+} r \frac{\partial W\left(r,n\right)}{\partial r} dr-\left(nk\right)^2 \int_{r_0^-}^{r_0^+} W\left(r,n\right) dr=\frac{\tau_0}{G_{\theta z}}\left[1+\left(-1\right)^{n+1}\right]\int_{r_0^-}^{r_0^+} r\,\delta(r-r_0) dr \tag{28}$$

Considering the fact that the displacements are continuous along the arc $r=r_0$ and making use of the integration by parts, Eq. (28) are simplified to

$$\frac{\partial W\left(r_0^+,n\right)}{\partial r}-\frac{\partial W\left(r_0^-,n\right)}{\partial r}=\left(\tau_0 / r_0 G_{\theta z}\right)\left[1+\left(-1\right)^{n+1}\right] \tag{29}$$

Application of conditions (29) to Eqs. (25) leads to

$$\left(C_2 r_0^{n\kappa}-D_2 r_0^{-n\kappa}\right)-\left(C_1 r_0^{n\kappa}-D_1 r_0^{-n\kappa}\right)=\left(\tau_0 / n\kappa r_0 G_{\theta z}\right)\left[1+\left(-1\right)^{n+1}\right] \tag{30}$$

The solution of Eqs. (27) and (30) results in the coefficients C_1, D_1, C_2 and D_2 and substituting of those into Eq. (25) and applying the inverse transform (5) to the ensuing equations leads to the displacement field as:

$$\begin{aligned} w\left(r,\theta\right)&=\frac{\tau_0}{\pi G G_{\theta z}}\sum_{n=1}^{\infty}\left(1+\left(-1\right)^{n+1}\right)\Gamma_n\left[\left(r r_0 / R_2^2\right)^{n\kappa}-\left(r / r_0\right)^{n\kappa}+\left(R_1^2 / r r_0\right)^{n\kappa}\right. \\ &\left.-\left(R_1^2 r_0 / R_2^2 r\right)^{n\kappa}\right]\cos\frac{n\pi\theta}{\alpha},\quad R_1 \le r \le r_0 \\ w\left(r,\theta\right)&=\frac{\tau_0}{\pi G G_{\theta z}}\sum_{n=1}^{\infty}\left(1+\left(-1\right)^{n+1}\right)\Gamma_n\left[\left(r_0 r / R_2^2\right)^{n\kappa}-\left(R_1^2 r / R_2^2 r_0\right)^{n\kappa}+\left(R_1^2 / r_0 r\right)^{n\kappa}\right. \\ &\left.-\left(r_0 / r\right)^{n\kappa}\right]\cos\frac{n\pi\theta}{\alpha},\quad r_0 \le r \le R_2 \end{aligned} \tag{31}$$

where $\Gamma_n=1/n\left(1-\left(R_1/R_2\right)^{2n\kappa}\right)=\Lambda_n/\sin(n\pi\beta/\alpha)$. Stress components in the whole region are attained in view of the constitutive Eqs. (2) as follows:

$$\tau_{rz}(r,\theta)=\frac{\tau_0}{G^2\alpha r}\sum_{n=1}^{\infty}n(1+(-1)^{n+1})\Gamma_n[\left(r_0r/R_2^2\right)^{n\kappa}-(r/r_0)^{n\kappa}-\left(R_1^2/r_0r\right)^{n\kappa}$$
$$+(R_1^2r/R_2^2r_0)^{n\kappa}]cos\frac{n\pi\theta}{\alpha},\quad R_1\le r\le r_0$$
$$\tau_{\theta z}(r,\theta)=-\frac{\tau_0}{G\alpha r}\sum_{n=1}^{\infty}n(1+(-1)^{n+1})\Gamma_n[\left(r_0r/R_2^2\right)^{n\kappa}-(r/r_0)^{n\kappa}+\left(R_1^2/r_0r\right)^{n\kappa} \tag{32}$$
$$-(R_1^2r_0/R_2^2r)^{n\kappa}]sin\frac{n\pi\theta}{\alpha},\quad R_1\le r\le r_0$$

For $r_0\le r\le R_2$ the stress component $\tau_{\theta z}(r,\theta)$ is achieved by replacing r/r_0 with r_0/r. Analogously for stress component $\tau_{rz}(r,\theta)$ similar changes are done for each region. Moreover the changed terms will be multiplied by negative sign. The term $n\Gamma_n$ is replaced by the series $\sum_{m=0}^{\infty}(R_1/R_2)^{2mn\kappa}$ and the stress components are summed up through the use of relations given in Appendix of [8].

$$\tau_{rz}(r,\theta)=\frac{\tau_0}{2G^2\alpha r}\sum_{m=0}^{\infty}[\psi_m\left(r_0r/R_2^2,\pi-\pi\theta/\alpha\right)-\psi_m\left(r_0r/R_2^2,\pi\theta/\alpha\right)$$
$$-\psi_m\left(r/r_0,\pi-\pi\theta/\alpha\right)+\psi_m\left(r/r_0,\pi\theta/\alpha\right)-\psi_m\left(R_1^2/r_0r,\pi-\pi\theta/\alpha\right)$$
$$+\psi_m\left(R_1^2/r_0r,\pi\theta/\alpha\right)+\psi_m\left(R_1^2r/R_2^2r_0,\pi-\pi\theta/\alpha\right)-\psi_m\left(R_1^2r/R_2^2r_0,\pi\theta/\alpha\right)],\quad R_1\le r\le r_0$$
$$\tau_{\theta z}(r,\theta)=-\frac{\tau_0}{2G\alpha r}\sum_{m=0}^{\infty}\{\varphi_m\left(r_0r/R_2^2,\pi\theta/\alpha\right)+\varphi_m\left(r_0r/R_2^2,\pi-\pi\theta/\alpha\right)-\varphi_m\left(r/r_0,\pi\theta/\alpha\right) \tag{33}$$
$$-\varphi_m\left(r/r_0,\pi-\pi\theta/\alpha\right)+\varphi_m\left(R_1^2/r_0r,\pi\theta/\alpha\right)+\varphi_m\left(R_1^2/r_0r,\pi-\pi\theta/\alpha\right)$$
$$-\varphi_m\left(R_1^2r_0/R_2^2r,\pi\theta/\alpha\right)-\varphi_m\left(R_1^2r_0/R_2^2r,\pi-\pi\theta/\alpha\right)\},\quad R_1\le r\le r_0$$

It can easily be seen that the displacement and stress fields satisfy the prescribed boundary and continuity conditions. For $R_1=0$ and $G_{\theta z}=G_{rz}$, Eqs.(33) are simplified and the stress field of reference [9] is achieved. The local coordinates $\left(r',\theta'\right)$, Fig. 1(b), is moved to the load location as $\theta=\sin^{-1}\left(r'sin\theta'/r\right),0\le\theta'\le\pi$ and $r=\sqrt{r'^2+r_0^2+2r'r_0cos\theta'}$. Using this transformation we deduce that $(\tau_{rz},\tau_{\theta z})\sim 1/r'$ near the traction τ_0 i.e. $r'\to 0$. Choosing a similar local coordinates in the sector corners it can be shown that the stress is not singular. These corners can be modeled by rectangular wedge apex which is not singular, confirming the report by [1] for isotropic wedges.

4 ORTHOTROPIC SECTOR WITH MULTIPLE CRACKS AND CAVITIES

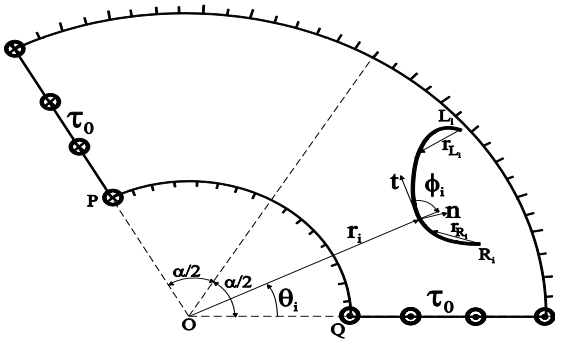

Fig.2
Schematic view of the sector with a smooth curved crack.

The dislocation solution accomplished in Section 3 may be extended to analyze sectors with multiple defects consist of cracks and cavities. The cavities are considered as closed-curve cracks without singularity. Consequently, the analysis resembles that of [8, 9] but with overriding the crack singularity. We consider a sector weakened by $r=r_0$ M cavities, $r=r_0$ N_1 embedded cracks, and $r=r_0$ N_2 edge cracks. Henceforth, we designate cavities, embedded cracks, and edge cracks with the respective subscripts as follows $i\in\{1,2,\ldots,M\}, j\in\{M+1,M+2,\ldots,M+N_1\}$, $k\in M+N_1+1,M+N_1+2,\ldots,M+N_1+N_2$ where $N=M+N_1+N_2$ and represents the total number of defects. The antiplane traction on the surface of the *i-th* defect, $i=1,2,\ldots,N$, Fig. 2, in terms of stress components in polar coordinates becomes

$$\begin{aligned}\tau_{tz}(r_i,\theta_i)&=\tau_{\theta z}(r_i,\theta_i)\sin\phi_i+\tau_{rz}(r_i,\theta_i)\cos\phi_i\\ \tau_{nz}(r_i,\theta_i)&=\tau_{\theta z}(r_i,\theta_i)\cos\phi_i-\tau_{rz}(r_i,\theta_i)\sin\phi_i\end{aligned}\tag{34}$$

where ϕ_i is the angle between tangent to the surface of the *i-th* defect and the radial direction r_i. Suppose dislocations with unknown density $B_{zj}(r_j)$ are distributed on the infinitesimal segment at the boundary of the *j-th* defect. The traction on the surface of the *i-th* defect due to the presence of the present distribution of dislocations, utilizing (34) and (18), leads to

$$\begin{aligned}\tau_{nz}(r_i,\theta_i)=&-\frac{B_{zj}(r_j)\kappa G_{rz}}{4\pi r_i}\sum_{m=0}^{\infty}\{\sin\phi_i\{\varphi_m(r_i/r_j,\pi(\theta_j-\theta_i)/\alpha)\\ &+\varphi_m(r_i/r_j,\pi(\theta_j+\theta_i)/\alpha)+\varphi_m(r_ir_j/R_2^2,\pi(\theta_j-\theta_i)/\alpha)+\varphi_m(r_ir_j/R_2^2,\pi(\theta_j+\theta_i)/\alpha)\\ &+\varphi_m(r_jR_1^2/r_iR_2^2,\pi(\theta_j-\theta_i)/\alpha)+\varphi_m(r_jR_1^2/r_iR_2^2,\pi(\theta_j+\theta_i)/\alpha)\\ &+\varphi_m(R_1^2/r_ir_j,\pi(\theta_j-\theta_i)/\alpha)+\varphi_m(R_1^2/r_ir_j,\pi(\theta_j+\theta_i)/\alpha)\}\\ &+G\{\psi_m(r_i/r_j,\pi(\theta_j+\theta_i)/\alpha)-\psi_m(r_i/r_j,\pi(\theta_j-\theta_i)/\alpha)+\psi_m(r_ir_j/R_2^2,\pi(\theta_j+\theta_i)/\alpha)\\ &-\psi_m(r_ir_j/R_2^2,\pi(\theta_j-\theta_i)/\alpha)-\psi_m(r_jR_1^2/r_iR_2^2,\pi(\theta_j+\theta_i)/\alpha)\\ &+\psi_m(r_jR_1^2/r_iR_2^2,\pi(\theta_j-\theta_i)/\alpha)-\psi_m(R_1^2/r_ir_j,\pi(\theta_j+\theta_i)/\alpha)\\ &+\psi_m(R_1^2/r_ir_j,\pi(\theta_j-\theta_i)/\alpha)\}\cos\phi_i\}\sqrt{(dr_j)^2+(r_jd\theta_j)^2};\quad R_1\le r_i\le r_j\end{aligned}\tag{35}$$

For $r_j\le r_i\le R_2$, the traction $\tau_{nz}(r_i,\theta_i)$ is written through the replacement of the term r_i/r_j by r_j/r_i and multiplying the functions ψ_m by a negative sign. Covering the boundary of cavities or border of cracks by dislocations, the principle of superposition may be brought into play to obtain traction on the surface of cavities or cracks. Equation set (35) is integrated on the boundary of defects and the resultant tractions are superimposed. The integration of Eq. (35) may be facilitated by describing the configuration of cracks and cavities in a parametric form. For example, the parameter $-1\le s\le 1$ is chosen and the following change of variables is employed for elliptical cavities with major and minor semi-axes a_i and b_i, respectively,

$$\begin{aligned}r_i(s)=&\{d_i^2+a_i^2b_i^2/[b_i^2\cos^2(\pi s+\omega_{si})+a_i^2\sin^2(\pi s+\omega_{si})]\\ &-2a_ib_id_i\cos(\pi s+\omega_{si}+\psi_{si})/\sqrt{b_i^2\cos^2(\pi s+\omega_{si})+a_i^2\sin^2(\pi s+\omega_{si})}\}^{\frac{1}{2}}\\ \theta_i(s)=&\tan^{-1}\{d_i\sin\beta_i\sqrt{b_i^2\cos^2(\pi s+\omega_{si})+a_i^2\sin^2(\pi s+\omega_{si})}\\ &-a_ib_i\sin(\pi s+\omega_{si}+\psi_{si}+\beta_i)/[d_i\cos\beta_i\sqrt{b_i^2\cos^2(\pi s+\omega_{si})+a_i^2\sin^2(\pi s+\omega_{si})}-a_ib_i\cos(\pi s+\omega_{si}+\psi_{si}+\beta_i)]\}\\ \phi_i(s)=&\tan^{-1}[r_i(s)\theta_i'(s)/r_i'(s)]\end{aligned}\tag{36}$$

where (d_i, β_i) is the coordinate of cavity center and $\phi_i(s)$ is the angle between a tangent to the surface of cavity and the radial direction $r_i(s)$. Also ω_{si} is the angle specifying the starting point and ψ_{si} is the orientation angle of the major axis. For more details, see [9]. In Eq. (36), prime designates differentiation with respect to the argument. The traction on the surface of the *i-th* crack or cavity in the sector containing *N* defects may be expressed as:

$$\tau_{nz}\left(r_i(s),\theta_i(s)\right)=\sum_{j=1}^{N}\int_{-1}^{1}b_{zj}(t)k_{ij}(s,t)dt \quad -1\le s\le 1, i=1,2,\ldots,N \tag{37}$$

where $b_{zj}(t)$ is the dislocation density on the non-dimensional length of the boundary of the *j-th* crack or cavity. The above kernel $k_{ij}(s,t)$ in light of Eq. (35) can be obtained as in the appendix. The functions $\varphi_0(r_i(s)/r_j(t),\pi(\theta_j-\theta_i)/\alpha)$ and $\psi_0(r_i(s)/r_j(t),\pi(\theta_j-\theta_i)/\alpha)$ are singular for $i=j$ as $t\to s$. Hence,we may conclude that $k_{ij}(s,t)$ has the Cauchy-type singularity for $i=j$ as $t\to s$. By virtue of Bueckner's principle, the left-hand side of Eq. (37), after changing the sign, is the traction caused by the external loading on the sector without defect at presumed boundary of cavities or crack border. The applied traction on sector with multiple defects is taken to be as Eq. (23) and the stress components as Eq. (33). Utilizing Eqs. (33) and (34), the following traction should be applied on the surface of the *i-th* defect:

$$\begin{aligned}
&\tau_{nz}\left(r_i(s),\theta_i(s)\right)=\frac{\tau_0}{2G^2\alpha r_i}\sum_{m=0}^{\infty}\{G[\varphi_m\left(r_0r_i/R_2^2,\pi\theta_i/\alpha\right)+\varphi_m\left(r_0r_i/R_2^2,\pi-\pi\theta_i/\alpha\right)\\
&-\varphi_m\left(r_i/r_0,\pi\theta_i/\alpha\right)-\varphi_m\left(r_i/r_0,\pi-\pi\theta_i/\alpha\right)+\varphi_m\left(R_1^2/r_0r_i,\pi\theta_i/\alpha\right)+\varphi_m\left(R_1^2/r_0r_i,\pi-\pi\theta_i/\alpha\right)\\
&-\varphi_m\left(R_1^2r_0/R_2^2r_i,\pi\theta_i/\alpha\right)-\varphi_m\left(R_1^2r_0/R_2^2r_i,\pi-\pi\theta_i/\alpha\right)]\cos\phi_i+[-\psi_m\left(r_0r_i/R_2^2,\pi-\pi\theta_i/\alpha\right)\\
&-\psi_m\left(r_0r_i/R_2^2,\pi\theta_i/\alpha\right)+\psi_m\left(r_i/r_0,\pi-\pi\theta_i/\alpha\right)+\psi_m\left(r_i/r_0,\pi\theta_i/\alpha\right)\\
&+\psi_m\left(R_1^2/r_0r_i,\pi-\pi\theta_i/\alpha\right)+\psi_m\left(R_1^2/r_0r_i,\pi\theta_i/\alpha\right)-\psi_m\left(R_1^2r_i/R_2^2r_0,\pi-\pi\theta_i/\alpha\right)\\
&-\psi_m\left(R_1^2r_i/R_2^2r_0,\pi\theta_i/\alpha\right)]\sin\phi_i\};\quad R_1\le r_i\le r_0\\
&\tau_{nz}\left(r_i(s),\theta_i(s)\right)=\frac{\tau_0}{2G^2\alpha r_i}\sum_{m=0}^{\infty}\{G[\varphi_m\left(r_0r_i/R_2^2,\pi\theta_i/\alpha\right)+\varphi_m\left(r_0r_i/R_2^2,\pi-\pi\theta_i/\alpha\right)\\
&-\varphi_m\left(R_1^2r_i/R_2^2r_0,\pi-\pi\theta_i/\alpha\right)-\varphi_m\left(R_1^2r_i/R_2^2r_0,\pi\theta_i/\alpha\right)+\varphi_m\left(R_1^2/r_0r_i,\pi\theta_i/\alpha\right)\\
&+\varphi_m\left(R_1^2/r_0r_i,\pi-\pi\theta_i/\alpha\right)-\varphi_m\left(r_0/r_i,\pi\theta_i/\alpha\right)-\varphi_m\left(r_0/r_i,\pi-\pi\theta_i/\alpha\right)]\cos\phi_i\\
&+[-\psi_m\left(r_0r_i/R_2^2,\pi-\pi\theta_i/\alpha\right)-\psi_m\left(r_0r_i/R_2^2,\pi\theta_i/\alpha\right)+\psi_m\left(R_1^2r_i/R_2^2r_0,\pi-\pi\theta_i/\alpha\right)\\
&+\psi_m\left(R_1^2r_i/R_2^2r_0,\pi\theta_i/\alpha\right)+\psi_m\left(R_1^2/r_0r_i,\pi-\pi\theta_i/\alpha\right)+\psi_m\left(R_1^2/r_0r_i,\pi\theta_i/\alpha\right)\\
&-\psi_m\left(r_0/r_i,\pi-\pi\theta_i/\alpha\right)-\psi_m\left(r_0/r_i,\pi\theta_i/\alpha\right)]\sin\phi_i\};\quad r_0\le r_i\le R_2
\end{aligned} \tag{38}$$

Employing the definition of dislocation density function, the equation for crack opening displacement across the *j-th* crack is

$$w_j^{+}(s)-w_j^{-}(s)=\int_{-1}^{s}\sqrt{(r_j'(t))^2+(r_j(t)\theta_j'(t))^2}\,b_{zj}(t)dt\ ,-1\le s\le 1, j=1,2,\ldots,N \tag{39}$$

The uniqueness requirement of displacement field on the surfaces of cavities and embedded crack borders implies

$$\int_{-1}^{1}\sqrt{(r_j'(t))^2+(r_j(t)\theta_j'(t))^2}\,b_{zj}(t)dt=0,\ j=1,2,\ldots,M+N_1 \tag{40}$$

The Cauchy singular integral Eqs.(37) and (40) are solved simultaneously to determine dislocation density functions. Cavities are defined as closed curved cracks with bounded dislocation density at both ends of cracks. Thus, for $-1 \le t \le 1, j = 1,2,\ldots,M$ the dislocation density functions for cavities are expressed as:

$$b_{zj}(t) = g_{zj}(t)\sqrt{1-t^2} \tag{41}$$

Stress fields for embedded cracks in orthotropic media are singular at crack tips with square root singularity ([16]).To show the order of stress singularity for embedded cracks located at the orthotropic sector, we chose a local coordinate (x, y) or (r', θ') as $x, y \to 0$ or $r' \to 0$, Fig. 1(b). Following, the transformation between the two coordinate systems (x, y) or (r, θ) is written as:

$$x = r\cos(\theta - \gamma) - d \qquad y = r\sin(\theta - \gamma) \tag{42}$$

Application of above transformation to Eq. (3) leads to

$$\begin{aligned}&(x+d)^2 \frac{\partial^2 w}{\partial x^2} + y^2 \frac{\partial^2 w}{\partial y^2} + 2y(x+d)\frac{\partial^2 w}{\partial x \partial y} + (x+d)\frac{\partial w}{\partial x} + y\frac{\partial w}{\partial y} \\ &+G^2[y^2 \frac{\partial^2 w}{\partial x^2} + (x+d)^2 \frac{\partial^2 w}{\partial y^2} - 2y(x+d)\frac{\partial^2 w}{\partial x \partial y} - y\frac{\partial w}{\partial y} - (x+d)\frac{\partial w}{\partial x}] = 0\end{aligned} \tag{43}$$

For $x, y \to 0$ the above equation is approximated by

$$\frac{\partial^2 w}{\partial x^2} + G^2 \frac{\partial^2 w}{\partial y^2} = 0 \tag{44}$$

Now let us make a comparison. We consider an orthotropic material where the shear modulus in the *x*-direction (G_{xz}) is different from that in the *y*-direction (G_{yz}). The governing equation of this material under anti-plane deformation is $G_{xz}\frac{\partial^2 w}{\partial x^2} + G_{yz}\frac{\partial^2 w}{\partial y^2} = 0$ [11]. The interesting thing is that we may be able to compare this equation with Eq. (44) by defining $G = \sqrt{G_{yz}/G_{xz}}$. The displacement field of orthotropic sector, which is globally governed by Eq. (3) by the coordinates (r, θ), is locally governed by Eq. (44). We recall that Eq. (44) is valid only for the infinitesimally neighborhood of point $A(r, \theta)$. Therefore in the vicinity of each specified point of the orthotropic sector we may assume an orthotropic material with the governing equation $G_{xz}\frac{\partial^2 w}{\partial x^2} + G_{yz}\frac{\partial^2 w}{\partial y^2} = 0$, but the material properties G_{xz} and G_{yz} should be replaced by G_{rz} and $G_{\theta z}$, respectively. We consider a crack tip located at the point (x, y) of an orthotropic sector $(G_{xz} \neq G_{yz})$. The displacement and stress distributions around the crack tip are given in the study by Liebowitz, Lee and Eftis [11] by solving the equation $G_{xz}\frac{\partial^2 w}{\partial x^2} + G_{yz}\frac{\partial^2 w}{\partial y^2} = 0$. For the brevity we give only the displacement field solution as:

$$w(x, y) = k_{III}\sqrt{2/G_{xz}G_{yz}}\, Im[\sqrt{x + (y/G)i}] \tag{45}$$

where $G = \sqrt{G_{yz}/G_{xz}}$ and k_{III} is the stress intensity factor of the tearing mode of fracture. The equation above is also valid for the infinitesimally neighborhood of each specified point of the orthotropic sector but the material

properties G_{xz} and G_{yz} are replaced by G_{rz} and $G_{\theta z}$, respectively. In view of Fig. 1(b) we have $x = r^{'}cos\theta^{'}$ and $y = r^{'}sin\theta^{'}$. Consequently, it is easy to deduce that the stress field in the crack tip has a square root singularity. Thus, the dislocation density functions are represented $-1 \le t \le 1, j = M+1,2,\ldots,M+N_1$ as:

$$b_{zj}(t) = g_{zj}(t)/\sqrt{1-t^2} \tag{46}$$

Following, Eq. (45) is rewritten for a crack tip located at the point $A(r,\theta)$ of the orthotropic sector, Fig. 1(b), as follows:

$$w(x,y) = k_{III}\sqrt{2/G_{rz}G_{\theta z}}\,Im[\sqrt{x+(y/G)i}\,] \tag{47}$$

Thus, the stress intensity factors for the *i-th* crack in terms of crack opening displacement are

$$k_{IIILi} = \frac{\sqrt{2}}{4}GG_{rz}\lim_{r_{L_i}\to 0}\frac{w^{+}(s)-w^{-}(s)}{\sqrt{r_{L_i}}}, k_{IIIRi} = \frac{\sqrt{2}}{4}GG_{rz}\lim_{r_{R_i}\to 0}\frac{w^{+}(s)-w^{-}(s)}{\sqrt{r_{R_i}}} \tag{48}$$

For $i = M+1,2,\ldots,N$, where *r* is the distance from a crack tip. Setting the points L_i and R_i on the surface of the crack, as shown in Fig. 2, yields

$$\begin{aligned} r_{L_i} &= \sqrt{(r_i(s))^2+(r_i(-1))^2-2r_i(s)r_i(-1)cos(\theta_i(s)-\theta_i(-1))} \\ r_{R_i} &= \sqrt{(r_i(s))^2+(r_i(1))^2-2r_i(s)r_i(1)cos(\theta_i(s)-\theta_i(1))} \end{aligned} \tag{49}$$

Substituting Eq. (46) into Eq. (39), substituting Eq.(49) into Eq. (48), and finally employing L'Hopital's rule yield the stress intensity factors for the embedded cracks:

$$\begin{aligned} k_{IIILi} &= \frac{1}{2}GG_{rz}[(r_i^{'}(-1))^2+(r_i(-1)\theta_i^{'}(-1))^2]^{\frac{1}{4}}g_{zi}(-1) \\ k_{IIIRi} &= -\frac{1}{2}GG_{rz}[(r_i^{'}(1))^2+(r_i(1)\theta_i^{'}(1))^2]^{\frac{1}{4}}g_{zi}(1) \end{aligned} \tag{50}$$

where $i = M+1,2,\ldots,M+N_1$. For edge cracks, taking the embedded crack tip at $t = -1$, for $-1 \le t \le 1$, $j = M+N_1+1, M+N_1+2,\ldots,N$, we let

$$b_{zj}(t) = g_{zj}(t)\sqrt{\frac{1-t}{1+t}} \tag{51}$$

Analogously, for an edge crack the stress intensity factor is

$$k_{IIILi} = GG_{rz}[(r_i^{'}(-1))^2+(r_i(-1)\theta_i^{'}(-1))^2]^{\frac{1}{4}}g_{zi}(-1) \tag{52}$$

where $i = M+N_1+1, M+N_1+2,\ldots,N$ .The anti-plane strain components on the surface of the *i-th* defect, $i = 1,2,\ldots,N$, Fig. 2, in terms of strain components in polar coordinates become

$$\begin{aligned} \gamma_{tz}(r_i,\theta_i) &= \gamma_{\theta z}(r_i,\theta_i)sin\phi_i+\gamma_{rz}(r_i,\theta_i)cos\phi_i \\ \gamma_{nz}(r_i,\theta_i) &= \gamma_{\theta z}(r_i,\theta_i)cos\phi_i-\gamma_{rz}(r_i,\theta_i)sin\phi_i \end{aligned} \tag{53}$$

Substituting strain components $\gamma_{rz}=\tau_{rz}/G_{rz}$ and $\gamma_{\theta z}=\tau_{\theta z}/G_{\theta z}$ into Eq. (53) and eliminating stress components τ_{rz} and $\tau_{\theta z}$ between the resultant equations and Eqs. (34) gives

$$\gamma_{tz}\left(r_i,\theta_i\right)=\left(\frac{cos^2\phi_i}{G_{rz}}+\frac{sin^2\phi_i}{G_{\theta z}}\right)\tau_{tz}\left(r_i,\theta_i\right)+\left(\frac{1}{G_{\theta z}}-\frac{1}{G_{rz}}\right)sin\phi_i cos\phi_i\,\tau_{nz}\left(r_i,\theta_i\right) \tag{54}$$

The calculation of hoop stress on the surface of cavities is accomplished by employing the definition of dislocation density function, i.e. $\gamma_{tz}\left(r_i\left(s\right),\theta_i\left(s\right)\right)=b_{zi}\left(s\right)$ and Eq. (54) and also using the fact that the *i-th* cavity surface is traction free $\tau_{nz}\left(r_i,\theta_i\right)=0$ as follows:

$$\tau_{tz}\left(r_i\left(s\right),\theta_i\left(s\right)\right)=\frac{G_{rz}G_{\theta z}}{G_{rz}sin^2\phi_i\left(s\right)+G_{\theta z}cos^2\phi_i\left(s\right)}b_{zi}\left(s\right),\quad -1\le s\le 1\qquad i=1,2,\ldots,M \tag{55}$$

The system of Cauchy integral Eq. (37) in conjunction with Eq. (40) can be solved numerically. To this end, the original numerical procedure developed by Erdogan, Gupta and Cook [17] may not be directly applicable since it does not consider all types of defects; i.e., embedded and edge cracks and also multiple cavities at the same time. In the study by Faal, Fariborz and Daghyani [18], a minor generalization of the numerical procedure, by means of expanding the continuous integrands of integral equations with different weight functions in terms of Chebyshoff and Jacobi polynomials, was introduced to overcome this problem. Various weight functions resulted from various stress fields of different types of crack tips and cavity boundaries. The only approximation in the modified method was the truncating integrand infinite expansion, which does not change the accuracy of results if an adequate number of discrete points are used (see, Faal [18] for more details).

5 NUMERICAL EXAMPLE AND DISCUSSIONS

The analysis framework developed in the preceding section allowed the consideration of an orthotropic sector with an arbitrary number of defects. These defects may contain embedded and edge cracks as well as cavities with different orientations. Let us consider a sector with $R_2=2R_1$ and a sector angle $\alpha=2\pi/3$. In the examples to follow, the orthotropy ratio *G* is assumed to be 0.8811 for an orthotropic material. For the isotropic case, *G*=1. The applied tractions are patch loads with the magnitude of τ_0 which are distributed on the sector straight edges, except for Example 4.

Example 1

Assume an orthotropic sector weakened by an elliptical cavity with major and minor semi-axes $a=0.3R_1$ and $b=0.1R_1$, respectively, Fig. 3. The center of cavity is on the line bisecting the sector at the distance $d=1.5R_1$. Fig.3 depicts the dimensionless hoop stress on the surface of the cavity for two different orientations of the cavity and also different materials (isotropic/orthotropic).The angle θ on the cavity is measured from the minor axis in the counter-clockwise direction. As can be seen in Fig. 3, the most severe hoop stresses are obtained at the sharpest points of the cavity. In the orthotropic sector, weaker material stiffness in the angular direction compared to that of the radial direction reduces the dimensionless hoop stress. For $\psi=0$, one of the sharpest points i.e. $\theta=\pi/2$ is in the minimum distance of the inner sector circular edge and has the global maximum hoop stress. Also other sharpest point at $\theta=3\pi/2$ has a local maximum hoop stress. For $\psi=\pi/2$ two sharpest points of cavity are in the identical distances of the sector bisector and have identical hoop stresses. One of the sharpest points of cavity i.e. $\theta=\pi/2$ for $\psi=0$ is closer than the distance from the point $\psi=\frac{\pi}{2}$ to the fixed edge of the sector, therefore the hoop stress of point $\theta=\pi/2$ for $\psi=0$ is higher than the one for $\psi=\pi/2$, Fig. 4 also shows the variation of non-dimensional hoop stress for point $\theta=3\pi/2$ of the cavity against the orientation angle ψ. Similarly, in the orthotropic sector,

the weaker material stiffness in the angular direction compared to that of radial direction reduces the dimensionless hoop stress. The problem is symmetric with respect to the angle $\psi = 0$ and $\psi = \pi$ as it can be seen in Fig. 4.

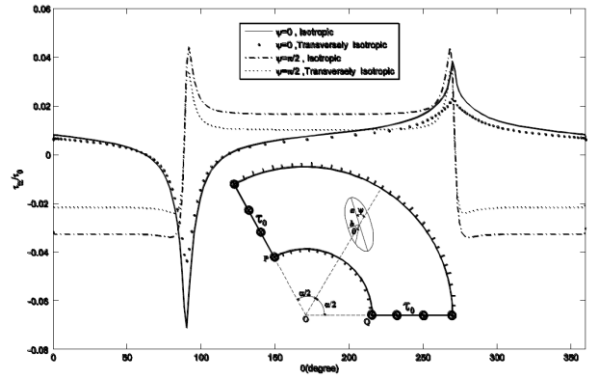

Fig.3
Dimensionless hoop stress for a cavity in an isotropic/orthotropic sector and two different cavity orientations.

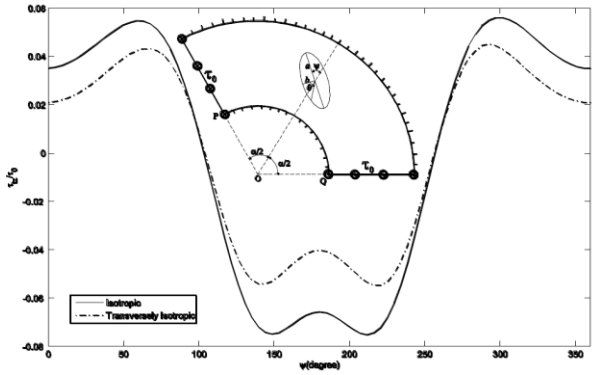

Fig.4
Variation of dimensionless hoop stress for point $\theta = \frac{3\pi}{2}$ of a cavity versus the orientation angle.

Example 2

The variation of hoop stress for two identical parallel axes cavities with centers at the distances $d_1 = 1.25R_1$ and $d_2 = 1.75R_1$ from the circular edges center is shown in Fig. 5. Minor axes of the cavities are on the line bisecting the sector. Also we have $a_1 = a_2 = 0.3R_1, b_1 = b_2 = 0.1R_1$ and the cavities orientation angle is $\psi_1 = \psi_2 = \frac{\pi}{2}$. Similar to the example with one cavity, the most severe hoop stresses are seen at the sharpest points of cavities or points with a maximum curvature. Moreover, the stress level of the isotropic sector is higher than the sector made of the orthotropic material, mainly because the material stiffness in the angular direction is weaker than that of the radial direction.

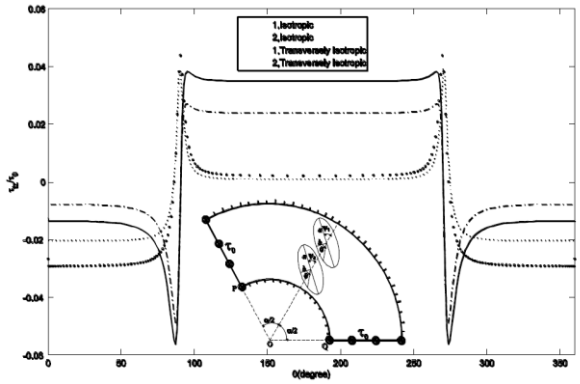

Fig.5
Dimensionless hoop stress for two cavities located at the sector with two different materials (isotropic/orthotropic).

Example 3

For this example let us consider two identical circular embedded cracks which are parallel with sector circular edges. The crack centers are fixed and located at the points $(1.5R_1, \pi/12)$ and $(1.5R_1, \pi/4)$. Fig. 6 shows the variations of non-dimensional stress intensity factors, k/k_0 at crack tips against l/R_1 where l is the half length of embedded circular cracks where $k_0 = \tau_0\sqrt{l}$. These cracks are located at an isotropic sector. The variation of stress intensity factor of crack tip R_2 is negligible whereas those near crack tips R_1, L_2 and also L_1 increase rapidly. In particular, for the tip L_1, the SIF increases because of approaching the loading point. Problem was solved again for an orthotropic sector and a similar trend was seen in Fig. 7. In the orthotropic sector, the weaker material stiffness in the angular direction increases the stress intensity factor. For two radial collinear cracks, one would envisage that it would behave reversely, which will be shown in Example 5.

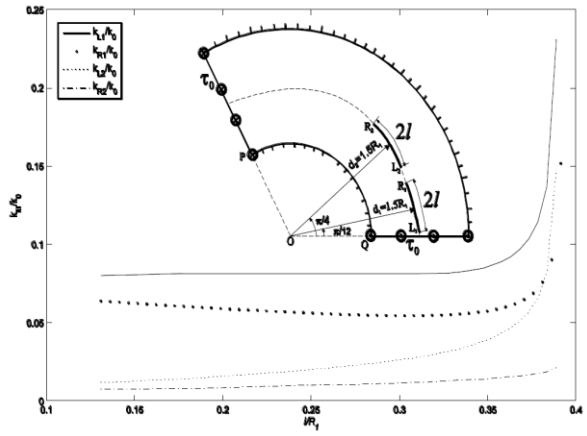

Fig.6
Variation of dimensionless stress intensity factor with l/R_1 for an isotropic sector.

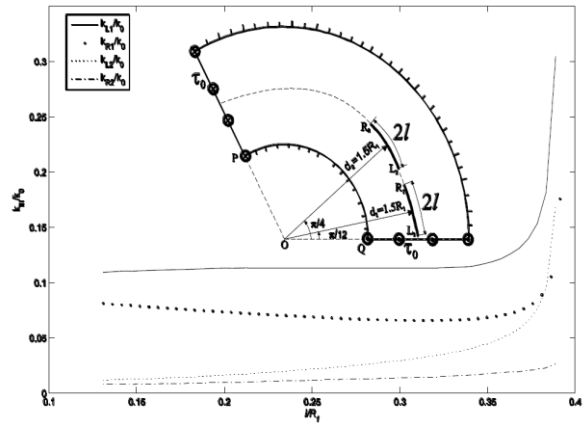

Fig.7
Variation of dimensionless stress intensity factor with l/R_1 for an orthotropic sector.

Example 4

Now we consider a sector weakened by a circular edge crack and an elliptical cavity with the length of major semi-axis $a = 0.3R_1$ and a minor semi-axis $b = 0.1R_1$. The major axis of the cavity is tangential to the circle with radius $1.5R_1$ at the point $(1.5R_1, \pi/4)$. The circular edge crack is parallel with the sector circular edges and in equal distances from the lower and upper boundaries. The patch loads are distributed on the sector straight edges except for the small gap with length $0.1R_1$ around the starting point of the edge crack. Fig.8 shows the dimensionless stress intensity factors, k/k_0, for the crack tipversus the dimensionless crack length l/R_1. For all crack lengths, the magnitude of SIF in the isotropic sector is higher than that of the orthotropic sector. As the crack tip approaches the sharpest point of the elliptical cavity, k/k_0 at the tip L increases rapidly. It is worth mentioning that when the

crack length grows up, SIF increases and when the crack tip recedes from the loading point, SIF deceases. In the mid points, depending on which of the aforementioned effects becomes dominant, SIF decreases or increases. The latter may explain the reason for the reduction of SIF in the middle portion of the plot in Fig. 9.

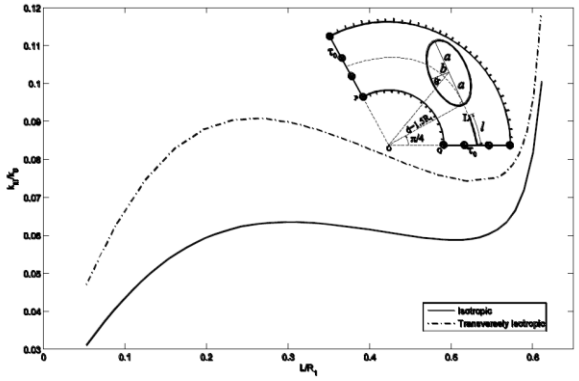

Fig.8
Variation of dimensionless stress intensity factor with l/R_1 for edge crack in a isotropic/orthotropic sector.

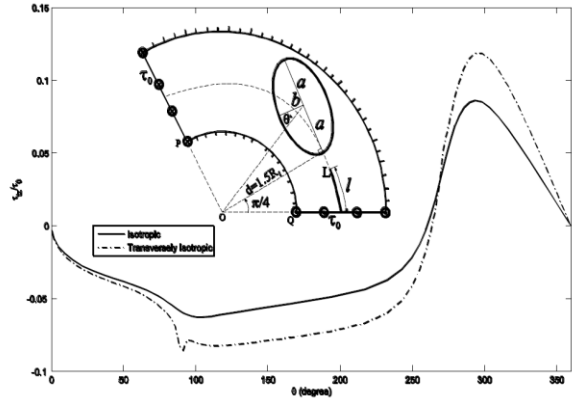

Fig.9
Variation of dimensionless hoop stress for a cavity in an isotropic/orthotropic sector.

Example5

This example contains a sector weakened by two equally-sized radial cracks bisecting the sector angle. The distance between the center of cracks is $0.5R_1$ and the distance from the center circular edges to the center of the first crack is $d_1 = 1.25R_1$. Figs.10 and 11 show the normalized stress intensity factors (SIF), k/k_0 of crack tips against l/R_1 where l is the half length of the embedded radial cracks. As can be seen from these figures, SIF increases rapidly as the distance between the tips of cracks decreases. The formation of regions with high stress level is attributed to the interaction of geometric singularities. Moreover, the slow reduction of other crack tips versus the crack length may be noteworthy. Interestingly, compared to the case in Example 3, an inverse trend is seen here in that the SIF for the isotropic sector is smaller than that of the orthotropic sector. For validation purposes, for an infinite wedge ($R_1 = 0$ and $R_2 \to \infty$) weakened by two equal-sized radial cracks bisecting the apex angle, we reexamined the solution procedure. The distances between the each crack center and wedge apex are $d_1 = l/10$ and $d_2 = 3l/10$, respectively, where the applied traction is patch load on the two wedge edges with the length $l = 0.1(m)$. The dimensionless stress intensity factors (k/k_0) determined by the present approach were found to be in excellent agreement with the results in Fig. 4 of the work by Faal et al. [8].

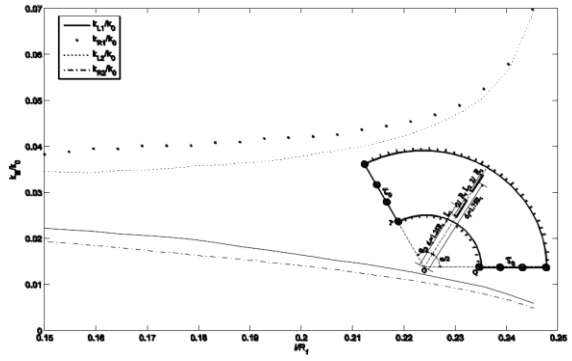

Fig.10
Variation of dimensionless stress intensity factor with l/R_1 for an isotropic sector.

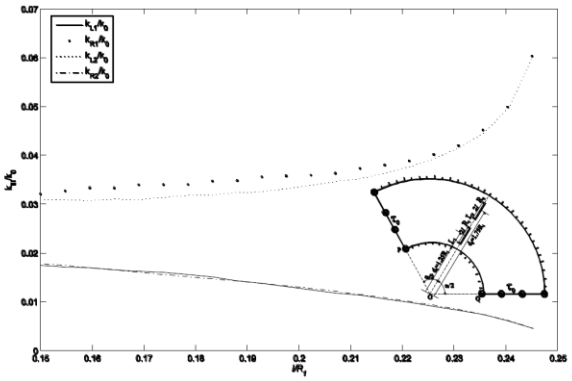

Fig.11
Variation of dimensionless stress intensity factor with l/R_1 for an orthotropic sector.

6 CONCLUSIONS

An analytical solution for the problem of orthotropic sectors weakened by Volterra-type screw dislocation was first obtained in terms of two new definite functions. Consequently, the stress field in an orthotropic sector under traction on its straight edge(s) was presented in a compact form, where the load and geometric singularity of stress field was shown. The dislocation density on the crack surfaces is obtainable by solving a set of integral equations of the Cauchy singular type. Finally, the distributed dislocation technique was used to solve problems with multiple cracks and cavities with smooth geometries. The presented examples on the embedded and edge cracks as well as cavities revealed that:

1. The normalized stress intensity factor (SIF) of the crack tips increases rapidly as they approach each other or near the sharp points of cavities or the loading point.
2. SIF at crack tips for both orthotropic $(G \neq 1)$ and isotropic $(G = 1)$ materials is symmetrically increased by an increase of the crack length. In the orthotropic sector, however, the weaker material stiffness in the angular direction reduces the stress intensity factor for radial collinear cracks and increases for circular cracks.
3. SIF of a crack tip that is closer to the sharpest point of the elliptical cavity increases as the crack approaches the cavity boundary. Also the largest value of dimensionless hoop stress is obtained at the points of cavity boundary with minimum curvature, which are at the nearest distances from the inner sector circular edges. The latter is because of the presence of regions with high stress concentration. A similar trend for the dimensionless hoop stress but with higher magnitude was observed on the cavity of the isotropic sector. Also SIF and hoop stress for finite wedge are obtained to be higher than those for a sector because of the singularity of finite wedge apex (for some apex angles), while the sector corners are not singular.

In Summary, the SIF of crack tips in orthotropic sectors can depend on critical factors such as the distance of the crack tip from the load, fixed edges or corners, and also the curvature of cavities. The individual and combined effects of these factors on SIF can be evaluated for different sector problems following the analytical solution provided in this work.

APPENDIX

Kernels of the integral equations

$$k_{ij}(s,t)=-\frac{\kappa G_{rz}}{4\pi r_i}\sum_{m=0}^{\infty}\{sin\phi_i\{\varphi_m(r_i/r_j,\pi(\theta_j-\theta_i)/\alpha)+\varphi_m(r_i/r_j,\pi(\theta_j+\theta_i)/\alpha)$$
$$+\varphi_m\left(r_i r_j/R_2^2,\pi(\theta_j-\theta_i)/\alpha\right)+\varphi_m\left(r_i r_j/R_2^2,\pi(\theta_j+\theta_i)/\alpha\right)+\varphi_m\left(r_j R_1^2/r_i R_2^2,\pi(\theta_j-\theta_i)/\alpha\right)$$
$$+\varphi_m\left(r_j R_1^2/r_i R_2^2,\pi(\theta_j+\theta_i)/\alpha\right)+\varphi_m\left(R_1^2/r_i r_j,\pi(\theta_j-\theta_i)/\alpha\right)+\varphi_m\left(R_1^2/r_i r_j,\pi(\theta_j+\theta_i)/\alpha\right)\}$$
$$+G\{\psi_m\left(r_i/r_j,\pi(\theta_j+\theta_i)/\alpha\right)-\psi_m\left(r_i/r_j,\pi(\theta_j-\theta_i)/\alpha\right)+\psi_m\left(r_i r_j/R_2^2,\pi(\theta_j+\theta_i)/\alpha\right)$$
$$-\psi_m\left(r_i r_j/R_2^2,\pi(\theta_j-\theta_i)/\alpha\right)-\psi_m\left(r_j R_1^2/r_i R_2^2,\pi(\theta_j+\theta_i)/\alpha\right)$$
$$+\psi_m\left(r_j R_1^2/r_i R_2^2,\pi(\theta_j-\theta_i)/\alpha\right)-\psi_m\left(R_1^2/r_i r_j,\pi(\theta_j+\theta_i)/\alpha\right)$$
$$+\psi_m\left(R_1^2/r_i r_j,\pi(\theta_j-\theta_i)/\alpha\right)\}cos\phi_i\}\sqrt{(r_j')^2+(r_j\theta_j')^2},\ R_1\le r_i\le r_j$$
$$k_{ij}(s,t)=-\frac{\kappa G_{rz}}{4\pi r_i}\sum_{m=0}^{\infty}\{sin\phi_i\{\varphi_m(r_i r_j/R_2^2,\pi(\theta_j-\theta_i)/\alpha)+\varphi_m(r_i r_j/R_2^2,\pi(\theta_j+\theta_i)/\alpha)$$
$$+\varphi_m\left(r_i R_1^2/r_j R_2^2,\pi(\theta_j-\theta_i)/\alpha\right)+\varphi_m\left(r_i R_1^2/r_j R_2^2,\pi(\theta_j+\theta_i)/\alpha\right)+\varphi_m\left(r_j/r_i,\pi(\theta_j-\theta_i)/\alpha\right)$$
$$+\varphi_m\left(r_j/r_i,\pi(\theta_j+\theta_i)/\alpha\right)+\varphi_m\left(R_1^2/r_i r_j,\pi(\theta_j-\theta_i)/\alpha\right)+\varphi_m\left(R_1^2/r_i r_j,\pi(\theta_j+\theta_i)/\alpha\right)\}$$
$$+G\{\psi_m\left(r_i r_j/R_2^2,\pi(\theta_j+\theta_i)/\alpha\right)-\psi_m\left(r_i r_j/R_2^2,\pi(\theta_j-\theta_i)/\alpha\right)$$
$$+\psi_m\left(r_i R_1^2/r_j R_2^2,\pi(\theta_j+\theta_i)/\alpha\right)-\psi_m\left(r_i R_1^2/r_j R_2^2,\pi(\theta_j-\theta_i)/\alpha\right)-\psi_m\left(r_j/r_i,\pi(\theta_j+\theta_i)/\alpha\right)$$
$$+\psi_m\left(r_j/r_i,\pi(\theta_j-\theta_i)/\alpha\right)-\psi_m\left(R_1^2/r_i r_j,\pi(\theta_j+\theta_i)/\alpha\right)$$
$$+\psi_m\left(R_1^2/r_i r_j,\pi(\theta_j-\theta_i)/\alpha\right)\}cos\phi_i\}\sqrt{(r_j')^2+(r_j\theta_j')^2},\ r_j\le r_i\le R_2$$

REFERENCES

[1] Kargarnovin M., Shahani A., Fariborz S., 1997, Analysis of an isotropic finite wedge under antiplane deformation, *International Journal of Solids and Structures* **34**: 113-128.

[2] Kargarnovin M., Fariborz S., 2000, Analysis of a dissimilar finite wedge under antiplane deformation, *Mechanics Research Communications* **27**: 109-116.

[3] Shahani A.R., 1999, Analysis of an anisotropic finite wedge under antiplane deformation, *Journal of Elasticity* **56**:17-32.

[4] Shahani A.R., 2003, Mode III stress intensity factors for edge-cracked circular shafts, bonded wedges, bonded half planes and DCB's, *International Journal of Solids and Structures* **40**: 6567-6576.

[5] Lin R.-L., Ma C.-C., 2004, Theoretical full-field analysis of dissimilar isotropic composite annular wedges under anti-plane deformations, *International Journal of Solids and Structures* **41**: 6041-6080.

[6] Chen C.-H., Wang C.-L., 2009, A solution for an isotropic sector under anti-plane shear loadings, *International Journal of Solids and Structures* **46**: 2444-2452.

[7] Mkhitaryan S.M., Melkoumian N., Lin B.B., 2001, Stress-strain state of a cracked elastic wedge under anti-plane deformation with mixed boundary conditions on its faces, *International Journal of Fracture* **108**: 291-315.

[8] Faal R., Fotuhi A., Fariborz S., Daghyani H., 2004, Antiplane stress analysis of an isotropic wedge with multiple cracks, *International Journal of Solids and Structures* **41**: 4535-4550.

[9] Faal R., Fariborz S., Daghyani H., 2007, Stress analysis of a finite wedge weakened by cavities, *International Journal of Mechanical Sciences* **49**: 75-85.

[10] Shahani A.R., Ghadiri M., 2010, Analysis of anisotropic sector with a radial crack under anti-plane shear loading, *International Journal of Solids and Structures* **47**:1030-1039.

[11] Liebowitz H., Lee J.D., Eftis J., 1978, Biaxial load effects in fracture mechanics, *Engineering Fracture Mechanics* **10**: 315-335.

[12] Faal R.T., Hassani A.R., Milani A.S., 2012, Stress analysis of transversely isotropic sectors weakened by multiple defects, *International Journal of Solids and Structures* **49**: 3627-3640.
[13] Faal R.T., Pasrad A., 2013, Stress analysis of two kinds of dissimilar isotropic sectors, *Mathematics and Mechanics of Solids* **18**: 543-555.
[14] Lekhnit͡skiĭ S.G., 1963, *Theory of Elasticity of an Anisotropic Elastic Body*, Holden-Day.
[15] Weertman J., Weertman J.R., Friedel J., Rhodes R.G., 1965, Elementary dislocation theory, tislocations and imperfections and active centers in semiconductors, *American Journal of Physics* **33**: 1091-1093.
[16] Delale F., 1984, Stress singularities in bonded anisotropic materials, *International Journal of Solids and Structures* **20**: 31-40.
[17] Erdogan F., Gupta G.D., Cook T.S., 1973, *Numerical Solution of Singular Integral Equations*, Springer Netherlands, Dordrecht.
[18] Faal R.T., Fariborz S.J., Daghyani H.R., 2006, Antiplane deformation of orthotropic strips with multiple defects, *Journal of Mechanics of Materials and Structures* **1**: 1097-1114.